

Optimizing mixing in lid-driven flow designs through predictions from Eulerian indicators

Kevin L. McIlhany, David Mott, Elaine Oran, and Stephen Wiggins

Citation: *Phys. Fluids* **23**, 082005 (2011); doi: 10.1063/1.3626022

View online: <http://dx.doi.org/10.1063/1.3626022>

View Table of Contents: <http://pof.aip.org/resource/1/PHFLE6/v23/i8>

Published by the American Institute of Physics.

Related Articles

High frequency dynamic bending response of piezoresistive GaN microcantilevers
Appl. Phys. Lett. **101**, 252102 (2012)

Light-addressable measurements of cellular oxygen consumption rates in microwell arrays based on phase-based phosphorescence lifetime detection
Biomicrofluidics **6**, 044118 (2012)

Low-frequency noise in gallium nitride nanowire mechanical resonators
Appl. Phys. Lett. **101**, 233115 (2012)

Focused ion beam milling and deposition techniques in validation of mass change value and position determination method for micro and nanomechanical sensors
J. Appl. Phys. **112**, 114509 (2012)

Nanoscale spatial resolution probes for scanning thermal microscopy of solid state materials
J. Appl. Phys. **112**, 114317 (2012)

Additional information on Phys. Fluids

Journal Homepage: <http://pof.aip.org/>

Journal Information: http://pof.aip.org/about/about_the_journal

Top downloads: http://pof.aip.org/features/most_downloaded

Information for Authors: <http://pof.aip.org/authors>

ADVERTISEMENT



**Running in Circles Looking
for the Best Science Job?**

**Search hundreds of exciting
new jobs each month!**

<http://careers.physicstoday.org/jobs>

physicstodayJOBS



Optimizing mixing in lid-driven flow designs through predictions from Eulerian indicators

Kevin L. McIlhany,^{1,a)} David Mott,^{2,b)} Elaine Oran,^{2,c)} and Stephen Wiggins^{3,d)}

¹*Physics Department, U. S. Naval Academy, Stop 9c, 572c Holloway RD, Annapolis, Maryland 21402-5002, USA*

²*Laboratories for Computational Physics and Fluid Dynamics, Naval Research Laboratory, Washington, DC 20375-5348, USA*

³*School of Mathematics, University of Bristol, University Walk, Bristol BS8 1TW, United Kingdom*

(Received 12 February 2011; accepted 27 June 2011; published online 19 August 2011)

In this paper, we further develop the notion of Eulerian indicators (EIs) for predicting Lagrangian mixing behavior. We employ a two-dimensional “blinking” Stokes flow as a model for mixing in a three-dimensional, spatially periodic channel flow. Each blinking flow alternates two distinct velocity fields that were calculated using a lid-driven cavity model. A new EI termed *mobility* is introduced to measure how effectively the blinking velocity fields transport fluid throughout the domain. We also calculate the transversality for these flows, which is an EI measuring how much the velocity direction at each point in the domain changes when the velocity fields blink. For the studied flows, we show that although individually the mobility and transversality do not correlate well with mixing as measured by the decay of the variance of concentration, the product of mobility and transversality does correlate well with the decay of the variance of concentration and predicts which combinations of velocity fields will produce the most effective mixing. © 2011 American Institute of Physics. [doi:[10.1063/1.3626022](https://doi.org/10.1063/1.3626022)]

I. INTRODUCTION

Many contemporary applications of fluid mechanics require precise knowledge and control of fluid elements and particle trajectories. This is particularly true at the micro- and nano-scales, where advances in fabrication capabilities are having a transformational impact on new and important applications in, e.g., manufacturing, medicine, and civil and military defense. These applications include hydrodynamic focusing for conductivity-based biosensors,¹ manipulating a sheath-core flow to manufacture polymer fibers,² and facilitating microflow cytometry.³ Fluidic components are critical parts of micro- and nano-scale systems that can be used for detecting chemical and biological agents and explosives, monitoring of the environment for hazardous chemicals or toxins, and diagnosing and treating medical problems. They can be used for transporting and mixing small amounts of materials that are subsequently analyzed or delivered to predetermined sites.

In this paper, we focus on mixing. Mixing is a very important step in many microfluidic applications, and mixing is also an area of significant interest in dynamical systems theory. In this paper, we merge the requirements of microfluidics and the techniques of dynamical systems theory to suggest component designs that enhance mixing.

The temporal and spatial requirements on fluidic components are complex, and so they often require the use of computational fluid dynamics (CFD) techniques in their analysis and design. CFD provides a description of the flow in terms

of the velocity field, given a fixed geometry and initial conditions. If information about transport phenomena such as mixing or surface delivery is required, then the particle trajectories generated by the velocity field are also required, which adds an additional layer of computational difficulty and expense to the problem.

Creating optimal designs for micro- and nano-fluidic components to achieve a desired task is daunting. Solving the partial differential equations for the velocity field, coupled with integrating the velocity fields to determine particle transport *for each candidate design*, stretches the limits of our capabilities when it is necessary for optimizing a design. A typical approach is to apply CFD techniques to analyze and improve incrementally an existing prototype by testing modest variations of the initial design.

The necessity of this incremental approach can be understood by considering the requirements of typical fluidic component design at the micro- and nano-scales. A typical requirement is to drive fluids in small channels that have etched or engraved geometric features, such as grooves at the bottom, the top, or both top and bottom of the channel. Such components can include hundreds of features, requiring millions of grid cells to model numerically. The analysis of a single user-specified design is practical, and if the design shows promise, then a limited parameter study that varies some aspect of the design through a small range may be performed. Given the large number of possible configurations, if arbitrary changes to the geometry and operating conditions are allowed, design and optimization over a wide parameter space, or *design space*, is impractical.

A general optimization computation can be accelerated in two ways. First, it can be accelerated by reducing the computational expense of modeling each individual design that is

^{a)}Electronic mail: mcilhany@usna.edu.

^{b)}Electronic mail: mott@lcp.nrl.navy.mil.

^{c)}Electronic mail: oran@lcp.nrl.navy.mil.

^{d)}Electronic mail: s.wiggins@bristol.ac.uk.

tested. Second, the large number of degrees of freedom associated with the design space can be reduced. One strategy, employed by the *computational toolbox* (CTB),⁴ exploits both of these approaches for designing microfluidic components. Designs are created by adding geometric features to a microchannel from a user-specified list of features. Transport data for each feature in isolation are precomputed and stored prior to the design calculation. During the optimization search, these data are retrieved and combined to predict the transport through arbitrary combinations of the features. The time required to characterize the flow through each design is reduced by several orders of magnitude relative to integrating the velocity fields during the optimization search.⁵ The complexity of the search is also reduced to determining the best sequence of features with pre-specified shapes, rather than the much more difficult task of optimizing an arbitrary geometric design. One constraint, which could be a limitation of this approach, is that the user must specify which features to include in the search. The features must be chosen such that the optimal design within the new restricted design space still provides good performance by some measure.

Rather than trying to accelerate the transport calculation, an alternative design approach avoids the transport calculations altogether. Since particle transport is determined by the velocity fields through which the particles move, direct analysis of these velocity fields can provide insights into the nature of the transport generated by combinations of these velocity fields. For the problem of mixing, *Eulerian indicators* (EIs) have been developed with the goal of predicting mixing characteristics based directly on the Eulerian velocity fields without calculating particle trajectories.⁶ EIs also provide a potential path for improving methods such as the CTB by providing guidance on which features should be included in the search library and in what sequence to combine these features. To date, application of EIs has been limited to assessing and predicting mixing characteristics of “blinking” type flows constructed from combinations of two or three distinct analytically defined velocity fields.⁷ At present, only two EIs have been studied extensively, α , the transversality (which will be discussed later), and β , the transverse shear.^{6,7}

In this paper, we continue our development of EIs by analyzing the mixing characteristics of a two-dimensional, lid-driven blinking Stokes flow. This flow serves as a model for mixing in a three-dimensional, spatially periodic, steady channel flow, where the blinking flow patterns model the two cross-sectional flow patterns that the fluid experiences as it moves down a spatially periodic channel. We begin by considering two EIs individually: the transversality (previously developed and studied in Refs. 6 and 7) and a new EI, called the *mobility*. While each EI does not necessarily correlate well with the mixing features of the flow (as determined by the decay of the variance of concentration), each does quantify a particular Eulerian feature of the flow that is an important component of the mixing process. The product of the two EIs, however, correlates well with the mixing characteristics of the flow. A discussion of the interpretation of the mobility and transversality, as well as the reason their product is considered, is given in Sec. IV.

We then describe the decay of the variance of concentration for two species of fluid that are initially segregated in

the domain. The variance of concentration serves as the mixing diagnostic for verifying the predictive capability of the EI. We then apply the techniques to the two dimensional lid-driven blinking flow. Overall, the main results are that the EIs, as a consequence of computational efficiency, allow us to obtain a picture of the mixing quality in the full design space of the blinking flow. As a result, for our flow model, parts of the design space that have been largely neglected by previous studies of the staggered herringbone mixer (SHM) yielded optimal designs that outperform more conventional designs.

II. BACKGROUND

It is important and useful to understand the nature of the relationship between the *Eulerian* problem of employing CFD techniques to solve for the velocity field and the *Lagrangian* problem of computing particle trajectories resulting from the velocity field. The Eulerian problem is *predictive* in nature. That is, CFD techniques compute the velocity field based on a chosen design, which includes geometrical and flow parameters, initial conditions, and boundary conditions, which can then be used to *predict* mixing performance. The Lagrangian problem of computing the trajectories of a collection of particles to analyze the appropriate transport problem is *retrodactive*, since the particle trajectories must first be computed (after the velocity field is computed) and then analyzed to characterize the mixing and transport processes.

In this paper, we consider the problem of mixing. The ideal solution would be to design the Eulerian problem of interest in a way that also solves the Lagrangian problem of interest, i.e., eliminate the need for the additional second step of computing particle trajectories and characterizing their behavior. Creating optimal mixing at the micro- and nano-scales is particularly challenging, since under typical flow conditions, the flow is laminar (i.e., there is no turbulent mixing), but the diffusion process, acting alone, is too slow for the desired applications. Therefore, our goal is to develop techniques that will enable us to design the velocity field (an Eulerian idea) in a way that optimizes mixing (a Lagrangian construct). This might appear to be overly optimistic since mixing and transport are fundamentally Lagrangian processes describing the relative displacement, over time, of fluid particles from their initial locations. Generally, the complexity generated by processes such as chaotic advection cannot be seen solely through examining the overall velocity field and its associated properties (e.g., shear).

With insight from the dynamical systems approach to Lagrangian mixing and transport, coupled with considerable intuition derived from experiments, several authors have proposed Eulerian quantities that characterize the promotion of “good mixing.”⁸ They observed that streamline crossing plays an important role in generating chaotic fluid particle trajectories. The two most common meanings of streamline crossing are

1. When instantaneous streamline patterns at two different times are superimposed, they “cross,” (the paradigm example here is the blinking vortex flow⁹).

2. For a steady, spatially periodic, three-dimensional flow, if the secondary flows in the cross-section at the beginning of a period and at half of a period are superimposed, their streamline patterns “cross” (the paradigm example here is the partitioned pipe mixer¹⁰).

Other authors¹¹ observed that “transversely oriented shears” played an important role in creating “good mixing.” The essential point is that in both of these papers (Lagrangian), mixing is related to a particular Eulerian observation.

There is a rigorous mathematical basis for understanding how these Eulerian characteristics promote mixing, and this comes from the theory of *linked twist maps* (LTMs). LTMs are one of the rare classes of dynamical systems for which one can rigorously prove the existence of the (mathematically) strongest possible mixing properties on the entire domain. The fundamental LTM theorems embody the Eulerian notions of streamline crossing and transversely oriented shears. Moreover, a number of “mixing scenarios” can be viewed within the framework of LTMs.^{12,13} As a historical note, it is perhaps useful to compare the notion of LTMs in mixing with that of Smale horseshoe maps. Smale horseshoes have played a fundamental role in developing a mathematical tool that embodies Reynolds’ early observation that stretching and folding are the key kinematic elements responsible for mixing in fluids.¹⁴ The chaos associated with the Smale horseshoe map, however, occurs rigorously on a set of zero area. Extensive numerical simulations must be carried out to discover the spatial extent of the influence of the Smale horseshoe on mixing (more retrodictive type analysis). In contrast, the LTM theorems can be viewed as proving the existence of dynamics similar to that of the Smale horseshoe, but on the entire domain.

The mathematical framework of LTMs (Refs. 8 and 11) motivated recent work⁶ which introduced EIs that quantified streamline crossing and transversely oriented shears for time-periodic, or steady spatially periodic flows. Such flows have two distinct patterns where streamline crossing and transversely oriented shears could be measured and quantified. The concept of EIs was further extended⁷ to the case of more than two distinct flow patterns and applied to a study of the optimization of mixing in a kinematic model of a channel flow.

The existing theorems that quantify the mixing properties of LTMs are not adequate for covering the wide variety of fluid flow situations where streamline crossing and transversely oriented shears occur, including those considered in this paper. While LTMs do embody the concepts of streamline crossing and transversely oriented shears, they include a geometrical condition on the two crossing streamline patterns that implies a (essentially Lagrangian) condition that forces all fluid particles to visit the regions of high streamline crossing and transversely oriented shear. EIs (Refs. 6 and 7) identify such regions in the flow, but outside of flow situations where the LTM theorems apply, we cannot guarantee that all (or even which) particles visit the regions of sufficiently high streamline crossing and transversely oriented shears. The new Eulerian indicator that we introduce, referred to as *mobility*, can be used to address this issue. For

the flows considered in this paper, the mobility is successful in the sense that the *product* of the two Eulerian indicators correlates well with the quality of mixing.

We apply these dynamical systems techniques to an analysis of the specific problem of mixing two streams of fluid moving down a channel of rectangular cross-section. This type of flow occurs in a fundamental fluidic component that plays a central role in a number of micro- and nano-fluidic applications. We assume that the two streams of fluid move according to the same *steady*, three-dimensional velocity field. If there is no component of velocity in the cross-section (i.e., transverse velocity components) then there is no mixing of the streams, except by molecular diffusion. Similarly, if the transverse velocity components are nonzero (and we are assuming steady), but are independent of the axial coordinate, then there is very poor mixing of the two streams. If the transverse velocity components depend upon the axial coordinate, however, then, as the two streams move down the channel, they can be stretched and folded among each other, which is the hallmark of chaotic mixing. In summary, as the fluid moves down the channel, it must experience a different cross-sectional velocity at different locations along the channel axis in order to mix well.

Over the past ten years, numerous groups have developed a variety of schemes for generating secondary flows in the cross-section for steady flows that promote mixing in microchannels. Perhaps, the most well-known scheme is the SHM.¹⁵ For this mixer, the flow is driven by a pressure gradient, and transverse components of velocity are created by a spatially periodic pattern of two types of herringbone shaped grooves in the bottom of the channel. The spatially periodic pattern of grooves insures that the fluid experiences two distinct cross-sectional flows *repeatedly* as it moved down the channel. The question arises; what geometry of the grooves is such that it generates optimal mixing?

This question has been addressed for the fully three-dimensional steady channel flow using computational fluid dynamics techniques.^{16–18} The computational effort required to address the full three-dimensional flow precluded a detailed analysis of the potential design space. Potentially, some study of the influence of additional parameters could be carried out by considering simpler models. Models of the SHM based on lid driven cavity flows have been considered,^{19–21} where walls with no-slip boundary conditions are moved in a way that simulates the secondary flows generated by the herringbone patterns, and the axial motion of the fluid is governed by an imposed pressure-driven Poiseuille flow.

A common feature of all of this work is that the flow pattern of the secondary flow in the cross-section contains two recirculation gyres divided by a separatrix extending from the top to the bottom of the channel. The location of the separatrix is fixed by the particular manner in which the secondary flow is created; either by the location of the elbow in the grooves on the bottom of the channel or in the manner in which the boundary of the cavity is moved. Moreover, the flows are spatially periodic in the sense that two distinct secondary flow patterns are experienced by the fluid as it moves down the channel. In the SHM mixer, as well as in the associated studies and models described above, a common

feature has been to position the separatrices of the two secondary flows *symmetrically* about the vertical line in the middle of the channel. In other words, they are horizontally reflected about the center.

A question that arises is whether or not more general types of secondary flows will lead to better mixing, i.e., more complete mixing in a shorter length of channel. Recent work⁷ with analytically derived velocity fields indicated that the best blinking-flow designs were *asymmetric*, meaning that the two separatrix locations were not related by a horizontal reflection about the channel centerline. Exploration of possible designs beyond modest parameter studies of a given prototype can be challenging using approaches based on traditional CFD or experiments. Fabricating micromixers and carrying out measurements on their mixing characteristics can be expensive and time consuming. Simulating micromixers using CFD techniques can also be expensive and time consuming. Both approaches require trial-and-error in order to develop geometries and methods for generating secondary flow patterns leading to optimal mixing. There is a need for a general framework and understanding of the kinematic issues required of the secondary flow structures that is *independent* of the particular manner in which the secondary flows are created, which is the subject of this paper.

In order to understand the specific nature of the two secondary flows on mixing, we considered a model that allows a variation of two secondary-flow structures. There are many possible parameters that one could consider, and vary, in any model. Here, we only consider two parameters; the locations of the two separatrices. A two-dimensional parameter space, or *design space*, is searched in order to determine the configuration(s) for which mixing is optimal. Each point in the design space requires the computation of a velocity field, and for each velocity field, a calculation of particle trajectories is performed for validation. The goal of using EIIs is to determine the points in the design space that will result in optimal mixing without the need to carry out the computationally expensive trajectory calculations, or, at the very least, limit the design space further by identifying velocity fields or combinations of fields that are ineffective for mixing.

III. TWO-DIMENSIONAL LID-DRIVEN STOKES FLOW MODEL AND THE DESIGN SPACE FOR BLINKING FLOW

In this section, we describe the lid-driven model that approximates the transverse velocity field in grooved three-dimensional channels, and we describe the resulting design space for a blinking flow that alternates between two of these velocity fields. Solving the Stokes equations numerically in a two-dimensional rectangular domain with moving boundaries can be done with many established methods and codes.²² Here, we just give sufficient details to describe the flows that we are considering.

A. Lid-driven two-dimensional Stokes flow model

We consider a rectangular domain with horizontal coordinate $-1.5 \leq y \leq 1.5$ and vertical coordinate $0 \leq z \leq 1$ (dimensionless units are used throughout). Zero velocity is

imposed on the side walls and ceiling, and the floor tangential velocity u_f is specified by

$$u_f = \begin{cases} \epsilon + 1.5 & \text{if } y < \epsilon \\ 0 & \text{if } y = \epsilon, \\ -(1.5 - \epsilon) & \text{if } y > \epsilon \end{cases} \quad (1)$$

with $-1.5 \leq \epsilon \leq 1.5$ indicating the location of the separatrix. We refer to this as an “In” configuration since the velocity vectors on the floor converge for $-1.5 < \epsilon < 1.5$ (for $\epsilon = \pm 1.5$, the flow matches a standard lid-driven cavity). The steady Stokes flow within this domain, driven by this imposed velocity on the floor, is then calculated using a pressure-correction method on a staggered grid.²²

Figure 1 shows streamlines and velocity magnitudes for the lid-driven model for $\epsilon = 0.5$. This choice sets $u_f = 2$ on the left $\frac{2}{3}$ of the channel floor, and $u_f = -1$ on the remaining $\frac{1}{3}$.

We also consider the case of diverging velocities on the floor (referred to as the “Out” configuration):

$$u_f = \begin{cases} -(\epsilon + 1.5) & \text{if } y < \epsilon \\ 0 & \text{if } y = \epsilon, \\ 1.5 - \epsilon & \text{if } y > \epsilon \end{cases} \quad (2)$$

The dependence of the wall velocity on the separatrix location was chosen to approximate the cross-sectional flow generated by herringbone-shaped grooves such as those used in the staggered herringbone mixer.¹⁵ The movement of the boundary corresponding to Eq. (1) generates a flow structure similar to the cross-sectional flow produced by a herringbone-shaped groove with the bend pointing downstream away from the channel entrance. Fluid in the two bottom corners meets at the separatrix after a time increment $\Delta t = 1$, which is analogous to the behavior of the three-dimensional structure. Similarly, movement of the boundary corresponding to Eq. (2) generates a flow similar to the cross-sectional flow generated by a herringbone-shaped groove with the bend pointing upstream toward the channel entrance. Fluid straddling the separatrix near the floor is split and delivered to the two bottom corners after a time increment $\Delta t = 1$, which is analogous to the behavior of the cross-sectional flow of the three-dimensional staggered herringbone mixer.

For the current study, velocity fields were computed for 51 values of ϵ ranging from $0 \leq \epsilon \leq 1.5$ in equally spaced

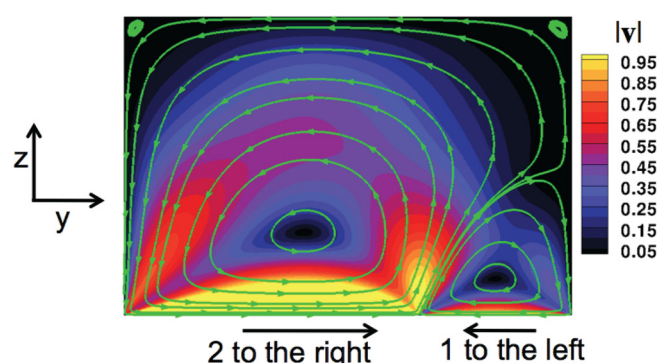


FIG. 1. (Color online) Velocity magnitude and streamlines for the lid-driven model with $\epsilon = 0.5$. Light gray (yellow online) indicates speeds ≥ 1 .

increments of 0.03. Reflections of these fields complete a set of 101 velocity fields ranging over $-1.5 \leq \epsilon \leq 1.5$.

B. Blinking-flow designs

Choosing a specific boundary movement, either Eq. (1) (“In”) or Eq. (2) (“Out”), and a value of ϵ specifies a velocity field. Choosing another value of ϵ and either the same or opposite boundary movement specifies another flow. A blinking flow is created by allowing the fluid to advect under the first flow (specified by, say, ϵ_1) for a specified time and then under the second flow (specified by, say, ϵ_2) for a specified time. This advection process is then repeated, indefinitely. In this way, we obtain a time-periodic blinking flow that blinks between the two flow patterns. This two-dimensional, time-periodic blinking flow is a model of the transverse flow patterns in the cross-section of three-dimensional, spatially periodic (steady) channel flow.

The space of all possible combinations of ϵ_1 and ϵ_2 is called the *design space* and is illustrated in Fig. 2. As an example of streamline crossing for two flow patterns (i.e., two distinct values of ϵ), Fig. 2 also shows streamlines for two specific fields ($\epsilon_1 = 0$ and $\epsilon_2 = 0.5$) and an overlay representing the design that combines these two. The velocity fields are applied in sequence for a prescribed number of cycles. In the results that follow, each field is applied for $\Delta t = 1$ before switching to the other field, and mixers were evaluated after a total of 15 cycles at $t = 30$.

We have computed velocity fields corresponding to 101 distinct values of ϵ for both the In boundary condition (defined by Eq. (1)) and the Out boundary condition (defined by Eq. (2)). If two In velocity fields are alternated to form the blinking flow, the configuration is referred to as “In-In.” If an In velocity field is alternated with an Out velocity field, the configuration is called “In-Out.” We will assess and compare the mixing characteristics of the 10 201 In-In and the 10 201 In-Out blinking flows that combine 101 choices for ϵ_1 with 101 choices for ϵ_2 .

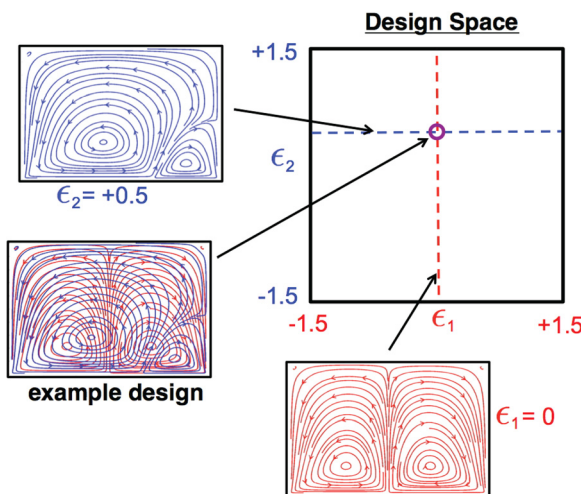


FIG. 2. (Color online) Design space of blinking-flow mixers using two alternating velocity fields. Values of ϵ_1 and ϵ_2 indicate the separatrix locations, and the streamlines correspond to the current lid-driven cavity model.

IV. PREDICTION OF MIXING: EULERIAN INDICATORS

In this section, we describe the Eulerian indicators and show how they can be used to quantify streamline crossing and mobility. We denote the two-dimensional velocity fields, with flow configuration parameter ϵ_i , by $\mathbf{v}(\mathbf{r}; \epsilon_i) = (u_y(y, z; \epsilon_i), u_z(y, z; \epsilon_i))$, $i = 1, \dots, N$, where N is the number of distinct flow configurations under consideration. The work in this paper is for $N = 2$. As a shorthand notation, the vector of parameters that define each flow configuration is $\epsilon \equiv (\epsilon_1, \dots, \epsilon_N)$, and the order of the ϵ_i in the vector is the order in which the different flow configurations are encountered in the blinking procedure. We denote the flow domain by \mathcal{D} (i.e., for our example, the rectangular domain defined in Sec. III) and the (N -dimensional) design space spanned by the ranges of the ϵ_i by \mathcal{P} .

A. Quantifying transversality (streamline crossing)

At each point $\mathbf{r} = (y, z)$ of the flow domain, we can associate an angle between velocity vectors associated with two adjacent flow configurations as

$$\alpha_{i,i+1}(\mathbf{r}) = \cos^{-1} \frac{\mathbf{v}(\mathbf{r}; \epsilon_i) \cdot \mathbf{v}(\mathbf{r}; \epsilon_{i+1})}{|\mathbf{v}(\mathbf{r}; \epsilon_i)| |\mathbf{v}(\mathbf{r}; \epsilon_{i+1})|}. \quad (3)$$

The subscript $i, i+1$ denotes the explicit dependence of the flow configuration parameters $\epsilon_i, \epsilon_{i+1}$, and “.” in the numerator denotes the scalar product of two vectors. Here, we do not take into account the direction of the velocity vectors. Since we are interested in the transversality of the two velocity vectors at a given point, we replace $\alpha_{i,i+1}(\mathbf{r})$ with

$$\hat{\alpha}_{i,i+1}(\mathbf{r}) = \begin{cases} \alpha_{i,i+1}(\mathbf{r}) & \text{if } 0 < \alpha \leq \pi/2 \\ \pi - \alpha_{i,i+1}(\mathbf{r}) & \text{if } \pi/2 < \alpha \leq \pi \\ \alpha_{i,i+1}(\mathbf{r}) - \pi & \text{if } \pi < \alpha \leq 3\pi/2 \\ 2\pi - \alpha_{i,i+1}(\mathbf{r}) & \text{if } 3\pi/2 < \alpha \leq 2\pi \end{cases},$$

so that $0 \leq \hat{\alpha}_{i,i+1}(\mathbf{r}) \leq \pi/2$ (see Figure 3).

Therefore, a measure of the cumulative degree of streamline crossing in the flow is given by

$$\hat{\alpha}(\mathbf{r}; \epsilon) \equiv \sum_{i=1}^N \hat{\alpha}_{i,i+1}(\mathbf{r}), \quad (4)$$

where N is cyclic ($N + 1 = 1$).

Finally, to produce a single number representing the degree of transversality associated with the N flow configurations, we average each $\hat{\alpha}_{i,i+1}(\mathbf{r})$ over the entire cross-section

$$\langle \hat{\alpha}_{i,i+1}(\mathbf{r}) \rangle_{\mathbf{r}} = \frac{\int_{\mathcal{D}} \hat{\alpha}_{i,i+1}(\mathbf{r}) d\mathbf{r}}{\int_{\mathcal{D}} d\mathbf{r}}, \quad (5)$$

and add each transition of the flows together to obtain

$$\bar{\alpha}(\epsilon) \equiv \sum_{i=1}^N \langle \hat{\alpha}_{i,i+1}(\mathbf{r}) \rangle_{\mathbf{r}}. \quad (6)$$

B. Quantifying mobility

The EI for mobility, η , is a measure of the fraction of the domain that experiences effective transport. When

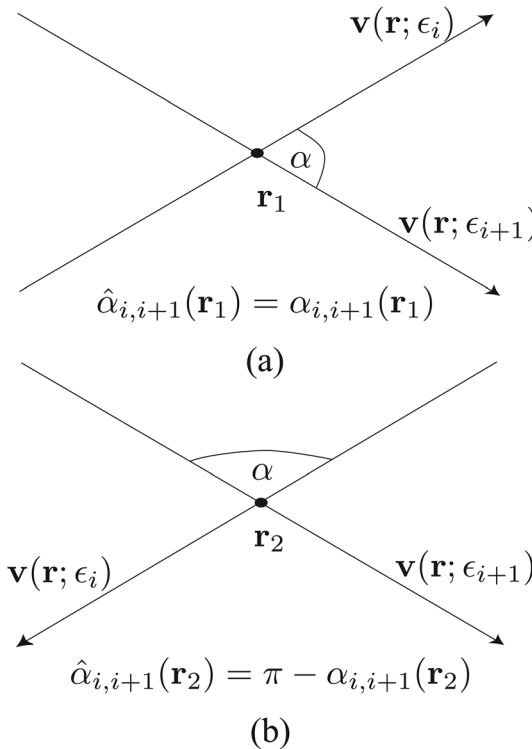


FIG. 3. Computation of $\hat{\alpha}_{i,i+1}(\mathbf{r})$. We disregard the direction of the velocity in this computation, so that in this figure, $\hat{\alpha}_{i,i+1}(\mathbf{r}_1) = \hat{\alpha}_{i,i+1}(\mathbf{r}_2)$.

regions within the flow field remain isolated and unmixed even as the bulk of the fluid mixes, one of the two primary mechanisms is likely involved. First, the flow pattern may create barriers to transport out of this region, such as when fluids follow a stable periodic or near-periodic path that requires the fluid to frequently return near its point of origin. Second, the average flow speed at points in this unmixed region may be very small relative to the average velocity magnitude in the domain. This can happen in blinking flows, even if the alternating velocity vectors at a particular point are not small, if these vectors are of nearly equal magnitude but point in opposite directions. The net effect over time in that region would be to “slosh” the fluid back and forth, with little net transport. Mobility quantifies this sloshing by comparing the percentage of the domain where points in the flow field experience poor transport due to low average velocity at those points to locations in the domain with high transport.

Mobility also accounts for regions of the domain which are stagnant, with near zero velocity at all times, such as in the region near a gyre center or close to a boundary with no-slip conditions. Consider Figure 2. The overlay of the two velocity fields shows regions where the net effect of the vector fields lead to a net zero displacement, whereas other regions align such that they always transport particles in the same direction, reinforcing transport.

More precisely, mobility is defined as the fraction of a domain that has a net (summed) velocity magnitude greater than a specified threshold. In order to define mobility mathematically and apply it to blinking flow, we need to define several other quantities. First, the summed velocity field is calculated. Each blinking velocity field is weighted in this

sum by the time over which it acts in a single blinking cycle. The magnitude of this summed velocity is small for regions with the sloshing behavior or stagnant regions described above. More precisely,

$$\mathbf{v}_{\text{sum}}(\mathbf{r}, \epsilon) \equiv \sum_{i=1}^N t_i \mathbf{v}(\mathbf{r}, \epsilon_i), \quad (7)$$

where t_i is the time that the velocity field $\mathbf{v}(\mathbf{r}, \epsilon_i)$ advects particles. We next compute the magnitude of this vector as a function of position, $|\mathbf{v}_{\text{sum}}(\mathbf{r}, \epsilon)|$. The mobility is then the fraction of the domain for which $|\mathbf{v}_{\text{sum}}(\mathbf{r}, \epsilon)|$ is greater than a specified threshold value.

The threshold value used for this study is the spatial average of $|\mathbf{v}_{\text{sum}}(\mathbf{r}, \epsilon)|$ for our particular blinking design

$$\overline{v_{\text{sum}}(\epsilon)} = \langle |\mathbf{v}_{\text{sum}}(\mathbf{r}, \epsilon)| \rangle_{\mathbf{r}} \equiv \frac{\int_{\mathcal{D}} |\mathbf{v}_{\text{sum}}(\mathbf{r}, \epsilon)| d\mathbf{r}}{\int_{\mathcal{D}} d\mathbf{r}}. \quad (8)$$

Then, we average the resulting quantity over the space of all possible designs

$$\widetilde{v_{\text{sum}}} = \langle \overline{v_{\text{sum}}(\epsilon)} \rangle_{\epsilon} \equiv \frac{\int_{\mathcal{P}} \overline{v_{\text{sum}}(\epsilon)} d\epsilon}{\int_{\mathcal{P}} d\epsilon}. \quad (9)$$

The resulting value, $\widetilde{v_{\text{sum}}}$, is the quantity that characterizes which values of the summed velocity vector are considered high or low. The threshold speed can be set to some percentage of $\widetilde{v_{\text{sum}}}$, but here we simply take the average over the whole of the design space as the threshold

$$v_{\text{thresh}} = \widetilde{v_{\text{sum}}}. \quad (10)$$

We define the points in the domain with $|\mathbf{v}_{\text{sum}}(\mathbf{r}, \epsilon)| \geq v_{\text{thresh}}$ as the mobile points. These points are given by

$$\mathcal{M}(\epsilon) = \{ \mathbf{r} \in \mathcal{D} \mid |\mathbf{v}_{\text{sum}}(\mathbf{r}, \epsilon)| \geq v_{\text{thresh}} \}. \quad (11)$$

The indicator function, \mathbb{I} , that assigns the value 1 to points in the flow domain in $\mathcal{M}(\epsilon)$ and 0 to points not in $\mathcal{M}(\epsilon)$ is given by

$$\mathbb{I}_{\mathcal{M}(\epsilon)}(\mathbf{r}) \equiv \begin{cases} 1 & \text{if } \mathbf{r} \in \mathcal{M}(\epsilon) \\ 0 & \text{if } \mathbf{r} \in \mathcal{D} \setminus \mathcal{M}(\epsilon). \end{cases} \quad (12)$$

Finally, the mobility is defined as

$$\eta(\epsilon) \equiv \frac{\int_{\mathcal{D}} \mathbb{I}_{\mathcal{M}(\epsilon)}(\mathbf{r}) d\mathbf{r}}{\int_{\mathcal{D}} d\mathbf{r}}. \quad (13)$$

The mobility is a measure of the percentage of the region of points in the domain, \mathcal{D} , where $|\mathbf{v}_{\text{sum}}(\mathbf{r}, \epsilon)|$ is greater than the threshold. A high value of $\eta(\epsilon)$ corresponds to a flow configuration whose spatial domain, \mathcal{D} , has a high percentage of good transport regions and a low percentage of stagnant regions. A stagnant region either experiences insignificant velocities from both blinking fields or counter-acting velocities, i.e., nonzero blinking velocities whose vector sum is near zero.

C. Interpretation of Eulerian indicators definitions

Individually, each of the EIs defined in this section will be compared to the variance of concentration. In both cases,

transversality and mobility, the EIIs agree with the variance of concentration for regions of poor performance. Regions in the design space with poor mixing also show poor performance by the individual EIIs. However, regions of good mixing in the design space do not correlate to regions of high performance by either EIIs alone. The mobility and transversality measure different aspects of flows that contribute to good mixing, and a metric that combines the two was sought. Since larger values of each individual metric are desirable, the simplest combination to try is the scalar product $\bar{\alpha} \cdot \eta$. This product avoids the need to choose a scaling or weighting for $\bar{\alpha}$ and η , which would be necessary if the two were added to form a composite metric. The product provides the strongest mechanism for assigning a poor score to those regions of the design space that have a small value for either $\bar{\alpha}$ or η .

V. QUANTIFYING MIXING: VARIANCE OF CONCENTRATION

A diagnostic that quantifies the degree of mixedness of fluids after a given time interval is needed to evaluate the performance of EIIs in predicting mixing. There is a significant literature on this subject.²³ Here, we use the normalized variance of concentration.^{7,24,25} Consider a mixture of two separate fluids, which we designate red and blue. The relative concentration of red fluid in some subdomain at some later time is given by

$$c = \frac{\#\text{red}}{(\#\text{red} + \#\text{blue})}, \quad (14)$$

where $\#\text{red}$ and $\#\text{blue}$ denote the number of red particles and the number of blue particles, respectively, in this area of interest at that instant. The variance of concentration is used as a measure of the mixing in a region of space

$$\mathcal{V}(t) = \frac{1}{N_{\text{bins}}} \sum_{i=1}^{N_{\text{bins}}} (c_i(\mathbf{r}_i, t) - c_{\text{avg}})^2. \quad (15)$$

For this study, the fluids were initially separated in a left-right orientation. From an initially unmixed state, the variance of concentration decreases over time, indicating mixing has occurred. When the value of the variance of concentration reaches zero, each subdomain is fully mixed.

After simulating the decay of the variance for the 10 201 different blinking-flow configurations, we find that the general behavior observed for the decay of the variance of concentration is exponential. For a fraction of the flows discussed, however, the decay is delayed slightly. The delay stems from the fact that when the first separatrix is located near the center of the domain, the initial fluid arrangement can remain unmixed until the separatrix moves away from the center. Once the separatrix has moved away from the center, the exponential decay begins. To account for the range of behaviors for the full set of flows considered, the decay of the variance of concentration is fit from $6 < t_{\text{fit}} < 30$. The final time, $t_{\text{final}} = 30$ is chosen to be long enough that the onset of asymptotic behavior is observable.

The time-dependence of $\mathcal{V}(t)$ is fitted to the expression

$$\mathcal{V}(t) = (A - \text{bias})e^{-t/\tau} + \text{bias}, \quad (16)$$

where the parameter τ is the time constant for the decay of $\mathcal{V}(t)$, A is $\mathcal{V}(0)$, and bias is the long-time behavior of $\mathcal{V}(t)$. The bias term accounts for the fact that some flow configurations never mix well. Flows which exhibit large “islands,” i.e., regions that do not mix with their surroundings, are good examples of high-bias configurations. The parameters τ and bias provide an indication of the quality of mixing. The decay is fast whenever τ is low. If, however, the bias term is high, a low value of τ can give a false impression of fast mixing. In this case, the variance of concentration quickly decays from a high initial value A down to a high bias value. Such mixers quickly approach their asymptotic performance, but this performance is poor. Low τ is therefore not sufficient to indicate good mixing. A low value of bias indicates good mixing at very long times, but if coupled with a high value of τ , the mixing is slow. Small values of both τ and bias give the best mixing performance.

VI. RESULTS AND DISCUSSION

This section presents and discusses the results of the analysis of the mixing properties of the two-dimensional, lid-driven blinking Stokes flow described above. We first discuss the decay of the variance of concentration, and then the EIIs, $\bar{\alpha}(\epsilon)$ and $\eta(\epsilon)$, and their correlation with this decay. The calculations of the transversality, mobility, and their product for 10 201 designs (the In-In configuration alone) took approximately 1 min on a single core of a 2.66 GHz Intel Core i5 processor. Calculating the variance of concentration at $t = 30$ for the same 10 201 configurations using the CTB required approximately 7 min on 16 cores on two 2.67 GHz Intel Core i7 processors. The variance calculation was therefore two orders of magnitude more expensive than the EI calculation. For comparison, rather than using the precomputed advection maps of the CTB, a traditional approach was also used for a limited number of configurations. Calculating the species transport employing a Runge-Kutta integration of the velocity fields on a 2.33 GHz Intel Core i7 processor averaged 600 s per configuration, which is three orders of magnitude slower than the CTB approach and five orders of magnitude slower than the calculation of the EIIs. A summary of the computational costs is provided in Table I.

A. Variance of concentration

For each of the 10 201 In-In flow configurations, the variance of concentration as a function of time, up to $t = t_f = 30$, has been computed. The value of the variance of concentration at $t_f = 30$, $\mathcal{V}(t_f = 30)$ is used to sort the

TABLE I. Table of computational cost for the 10 201 “In-In” flow configurations. Tests performed on comparable but not identical processors (see text for details).

Calculation	CPU time (min)
EIIs	~1
Variance of concentration using CTB	112
Variance of concentration using Runge-Kutta to integrate streamline paths	~102 000 ^a

^aEstimate based on 1000 realizations within the design space.

TABLE II. In-In: Table of mixing quality and thresholds with respect to the decay of the variance of concentration for the “In-In” flow configurations.

Mixing quality	Percentage of values in range (%)	Range of $\mathcal{V}(t_f)$	Dot color	Qualitative description
Best	10	<0.033	White (yellow online)	Mixes fastest and most thoroughly
Good	20	0.033 → 0.045	Light gray (red online)	Mixes quickly and well
Medium	20	0.045 → 0.062	Dark gray (blue online)	Mixes to some degree
Poor	50	>0.062	Black	Mixes poorly, slowly, or both

different configurations into four sets of mixed states labeled best, good, medium, and poor. Table II shows the range of values for each classification of mixers based on this scheme for the In-In configuration. The best mixers comprise the top 10% of designs, good mixers are the following 20%, medium mixers comprise the next highest 20% of values, and the remaining 50% are poor mixers.

Figure 4 shows the variance of concentration at $t = 30$ for all 10 201 In-In configurations ranked from best to poor, and Figure 5 shows the variance of concentration as a function of time for these 10 201 blinking flows ordered in the same way. Figure 5 shows both the exponential decay of the variance of concentration over time and the initial delay in this decay in some configurations. This delay is evident in the plateau that appears at lower times before the more pronounced decay occurs. Figure 5 also demonstrates the need for the *bias* parameter to generate a fit of this decay for each design since the variance of concentration for the various designs do not approach the same value, much less uniformly approach zero, at the later times.

1. Tau (τ) and bias

The values of τ and *bias* (defined in Sec. V) were calculated from the variance of concentration histories for each of the blinking flow designs. The scatter plot of τ -*bias* shown in Fig. 6 indicates the values of these parameters and the quality of mixing for each design. Each colored dot represents a single flow configuration, defined in Sec. III B, and the dots are colored according to the criteria given in Table II.

Figure 6 shows the τ -*bias* plane for the In-In configurations, i.e., boundary motion defined by Eq. (1) for both fields. The best mixers populate the lower left-hand corner, where τ and *bias* are both low. Moving away from the lower left-hand corner are successively the good, then medium mixers. Poor mixers reside in the rest of the τ -*bias* space. Flow con-

figurations which have low *bias* values and high τ values are mixers which will eventually mix well, however slowly. Flow configurations with high *bias* values will never mix well, no matter the time length. These high-*bias* low configurations are associated with large island structures, i.e., regions that do not mix with the rest of the domain. Figure 10(c) illustrates an example of a high-*bias* configuration $(\epsilon_1, \epsilon_2) = (1.2, -1.2)$.

Figure 7 shows the τ -*bias* plane for the In-Out flow configuration where the first velocity field is directed inward along the moving boundary, towards the separatrix, followed by a second velocity field directed outward, away from the separatrix (i.e., boundary motion defined by Eq. (1) for the first field and Eq. (2) for the second field). The color for each dot indicates how that design ranked compared to the other In-Out designs based on $\mathcal{V}(t_f = 30)$, and Table III shows the range of values for each classification for the In-Out configuration. As with the In-In configurations, good mixers have low values for both τ and *bias*. Poor mixers have high values for τ , *bias*, or both.

Tables II and III demonstrate that the In-In mixers outperform the In-Out mixers. The values of variance of concentration separating the various categories from best to poor are higher for the In-Out configuration than the In-In configuration. This fact is reflected in Figs. 6 and 7 as well. For each category of mixers based on mixing quality, both τ and *bias* for the In-Out configurations reach higher values than the same category for the In-In mixers, which indicates slower and less-complete mixing for the In-Out designs. Furthermore, the fastest decays occur for the In-In configurations, where τ reaches a minimum near 8.0, as can be seen in the inset for Figure 6 compared to the fastest decays for the In-Out configurations whose minimum tau value reaches only 9.5, seen in the inset of Figure 7. These studies show

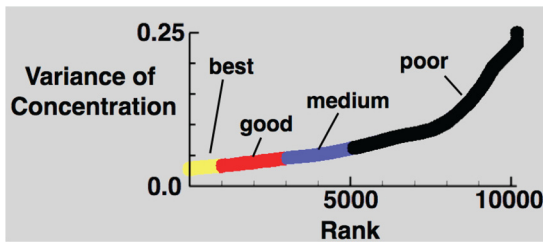


FIG. 4. (Color online) In-In: Variance of concentration, $\mathcal{V}(t_f = 30)$, with the set of flow configurations sorted from lowest to highest variance. The quality of mixing determination is indicated by partitioning the configurations into the lowest 10% (best), next 20% (good), next 20% (medium), and the final 50% (poor).

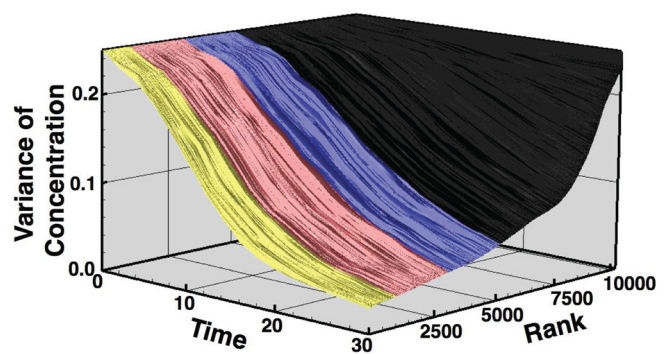


FIG. 5. (Color online) In-In: Variance of concentration, $\mathcal{V}(t)$, versus time [0, 30] versus the set of flow configurations. Note the initial time delay exhibited by some configurations.

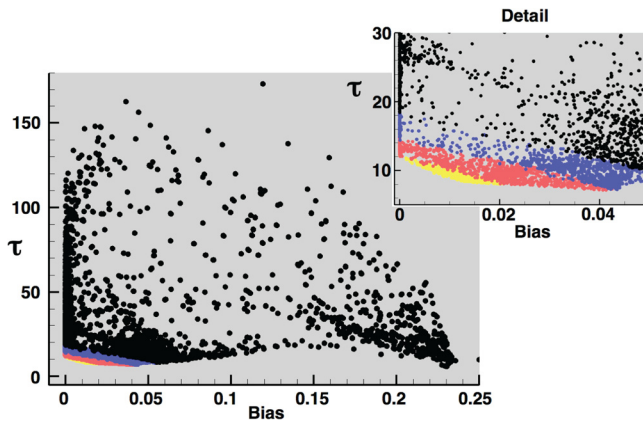


FIG. 6. (Color online) In-In: τ versus bias for the set of flow configurations where the velocity vectors point inward towards the separatrices for both vector fields.

that the In-In designs are systematically better than the In-Out designs for the two dimensional lid-driven design space.

2. Comparison of Eulerian indicators and final variance of concentration

Figures 8 and 9 show a comparison between the EIIs and the quality of mixing throughout the design space for the In-In and In-Out flow configurations, respectively. In order to compare surfaces of EIIs to the quality of mixing, colored dots are used for the four broad classes of mixing defined in Table II. The variance of concentration is shown in Fig. 8(c), the product of $\alpha \cdot \eta$ is shown in Fig. 8(d) with colored dots from Fig. 8(c) overlaid. First, note that the contours of transversality, $\bar{\alpha}(\epsilon_1, \epsilon_2)$, and mobility, $\eta(\epsilon_1, \epsilon_2)$, individually correlate to the quality of mixing only by a marginal amount. The product of transversality and mobility, however, correlates well with quality of mixing. For both the In-In and In-Out configurations, the best designs based on $\mathcal{V}(t_f = 30)$ are asymmetric in that they combine a field with ϵ near one of the extremes (± 1.5) with a field near $\epsilon = 0$, but offset slightly from the center of the channel (typically $|\epsilon| < 0.5$). For the In-In case, ϵ_1 and ϵ_2 have the same sign for the best mixers. For the In-Out case, ϵ_1 and ϵ_2 have opposite signs for the best mixers. The product metric captures this extreme in both cases within bands of high values of $\bar{\alpha} \cdot \eta$.

The definition of $\bar{\alpha}$ depends upon the crossing angle of the alternating streamline patterns and not on which direction the velocity is directed along the streamlines. The In-oriented velocity field at a particular value of ϵ has identical streamline paths as the Out-oriented field at the same ϵ , although the sign on the velocity is opposite between the two

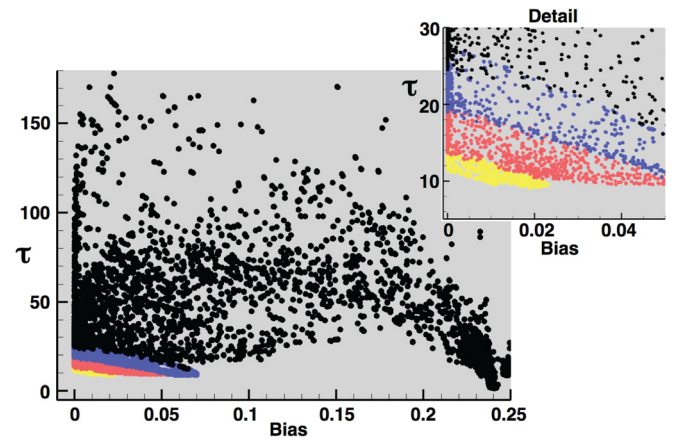


FIG. 7. (Color online) In-Out: τ versus bias for the set of flow configurations where the velocity vectors point inward towards the separatrix for the first vector field and outwards, away from the separatrix for the second vector field.

orientations. A consequence of this fact is that the transversality results (Figs. 8(a) and 9(a)) are identical for In-In and In-Out designs.

For the In-In configurations, the mobility is relatively high for designs with $\epsilon_1 = \epsilon_2$ because at each point in the domain the two identical velocity fields always act in the same direction. The mobility is highest in the In-In configurations for $\epsilon_1 = \epsilon_2 = \pm 1.5$ since the wall velocity is highest when the separatrix is pushed completely to one of the boundaries. The mobility is lowest for $\epsilon_1 = -\epsilon_2 = \pm 1.5$ because the two velocity fields sum to zero, which generates no net flow. For the In-Out configurations, the designs with $\epsilon_1 = \epsilon_2$ produce low mobility due to this canceling effect of the alternating velocity fields, and high mobility is seen for $\epsilon_1 = -\epsilon_2 = \pm 1.5$ where the two velocity fields reinforce each other.

Studies of the SHM to date have focused on the symmetrical placement of the separatrix, reflected horizontally about $x=0$. In the design spaces shown in Figures 8 and 9, the symmetrical designs correspond to the set of designs forming a diagonal line running from the upper left-hand corner down to the lower right-hand corner. This study shows that for the two-dimensional, lid-driven blinking Stokes flow, the symmetric blinking configurations do not mix as well as the asymmetric configurations. We note that the symmetric blinking configurations model the cross sectional flow of the SHM. These results indicate a possible improvement to the design of the SHM that will enhance mixing. The result was also demonstrated in previous work⁷ for a kinematically defined velocity field. In that case, the result was attributed to a “scraping” phenomena at the wall when the separatrix was placed near the wall. Although the no-slip condition was

TABLE III. In-Out: Table of mixing quality and thresholds with respect to the decay of the variance of concentration for the “In-Out” flow configurations.

Mixing quality	Percentage of values in range (%)	Range of $\mathcal{V}(t_f)$	Dot color	Qualitative description
Best	10	<0.041	White (yellow online)	Mixes fastest and most thoroughly
Good	20	0.041 → 0.066	Light gray (red online)	Mixes quickly and well
Medium	20	0.066 → 0.088	Dark gray (blue online)	Mixes to some degree
Poor	50	>0.088	Black	Mixes poorly, slowly, or both

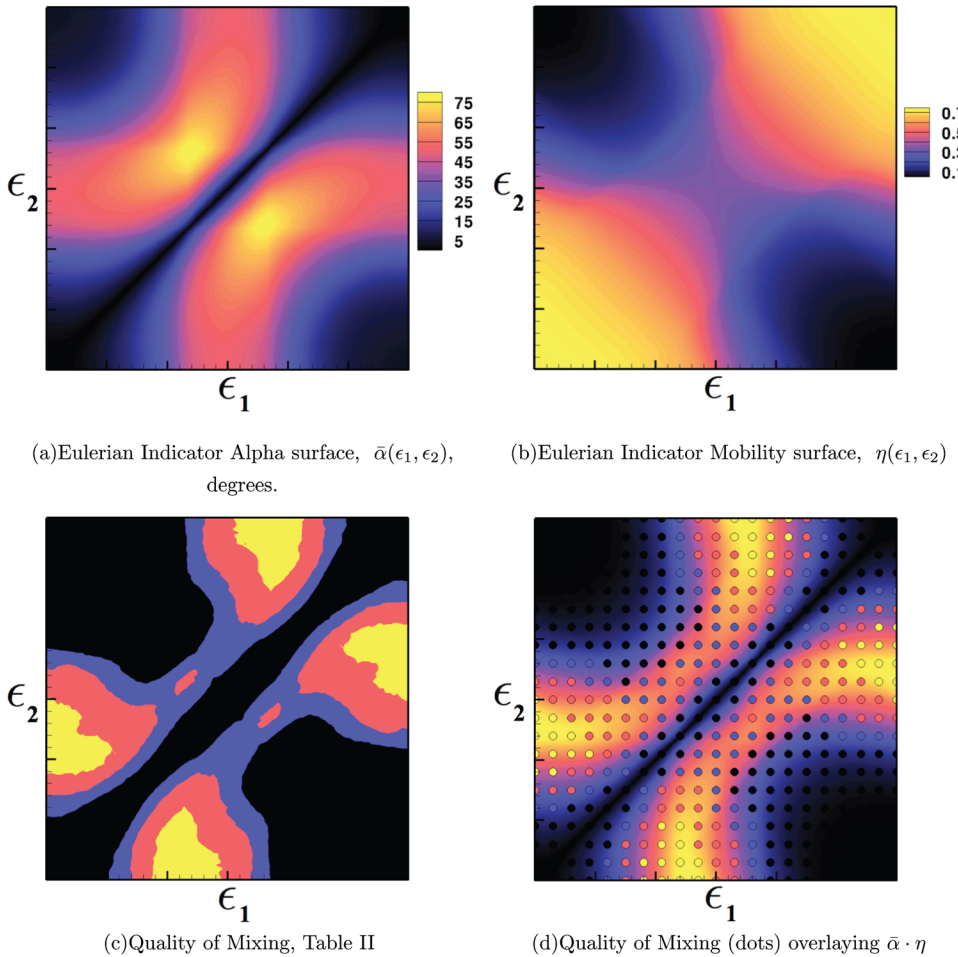


FIG. 8. (Color online) In-In: Eulerian metrics and quality of mixing based on variance of concentration for the blinking-flow design space. The lid-driven velocity fields rotate such that the velocity vectors point inward toward the center of the domain for both vector fields.

still imposed, transport near the wall was enhanced by squeezing the adjacent gyre closer to the wall. The dynamics of the current lid-driven model are significantly different from this previous study but yield a similar result. As the separatrix is placed closer to the wall for the lid-driven model, the gyre adjacent to the wall becomes smaller and weaker, and the larger gyre begins to engage more and more of the domain. With the separatrix placed at the wall, the smaller, weaker gyre vanishes and the entire side wall is exposed to the larger, stronger vortex. Placing the separatrix near one of the side walls therefore provides the best transport along the walls. Choosing a second field that places the separatrix near the centerline generates high transversality, another condition that leads to good mixing. By satisfying both conditions, the best mixing configurations are found at positions in the design space near $(\epsilon_1, \epsilon_2) = (0, \pm 1.5)$ or $(\pm 1.5, 0)$ which can be seen in Figures 8 and 9.

3. Simulation of tracer evolution

Now that the mixing characteristics of the design space have been determined, we examine the evolution of tracers for representative designs. Figure 10 shows the distribution of two species, darker (blue online) and lighter (red online), at $t = 10$ (top row) and $t = 30$ (middle row), and Poincare sections (bottom row), for three representative In-In mixers: one good mixer, one poor mixer with good mobility but low

transversality, and one mixer with both poor mobility and poor transversality. The distributions were calculated using the CTB. The initial condition considered here for the species concentrations consists of all darker-gray fluid starting in the left half and all lighter fluid starting in the right half of the rectangular domain. For calculating the Poincare sections, 20 particles were seeded equally spaced along the mid-height ($y = 0.5$) of the domain and advected for 10 000 cycles.

The good design, $(\epsilon_1, \epsilon_2) = (1.2, 0.3)$, lies within one of clusters of peak values in Fig. 8. This combination effectively pumps fluid from the corners toward the center of the domain, and then up toward the roof, while simultaneously interlacing the two species and eliminating most of the large islands of either species. In contrast, the mixer with $(\epsilon_1, \epsilon_2) = (-1.5, -1.5)$ generates a large single gyre that does not break the two fluids into smaller regions. The two species remain in two continuous regions that are slowly stretched and wound around each other. Large regions near the walls, and a smaller island in the center of the gyre, are poorly populated in the Poincare plot. Finally, the design with $(\epsilon_1, \epsilon_2) = (1.2, -1.2)$ is very inefficient, largely sending fluid at the bottom of the domain back and forth along the floor without generating a larger-scale flow away from the floor. The Poincare section for this case shows that large islands of the two species rotate slowly but do not mix. This rotation is not visible in the species plots due to the side-by-side arrangement of the initial species distributions.

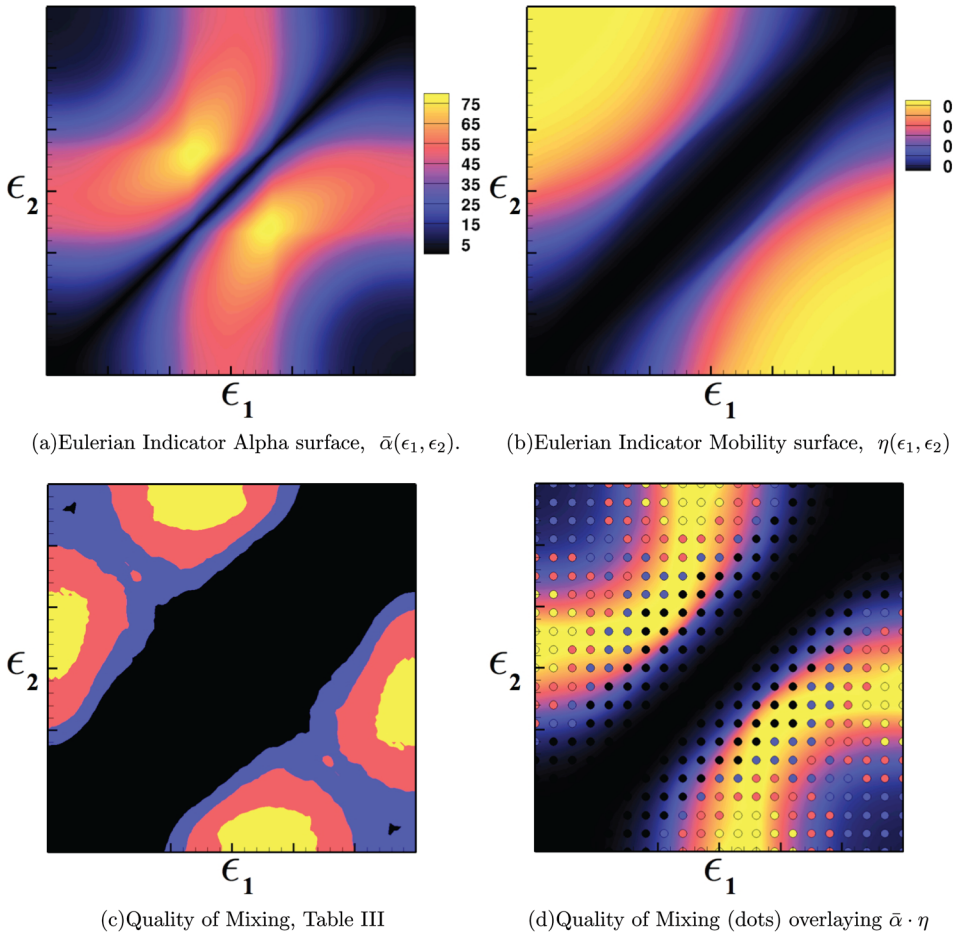


FIG. 9. (Color online) In-Out: Eulerian metrics and quality of mixing based on variance of concentration for the blinking-flow design space. The lid-driven velocity fields rotate such that the first velocity vector field points inward along the bottom, towards the separatrix followed by the second velocity vector field, which points outward, away from the separatrix along the bottom.

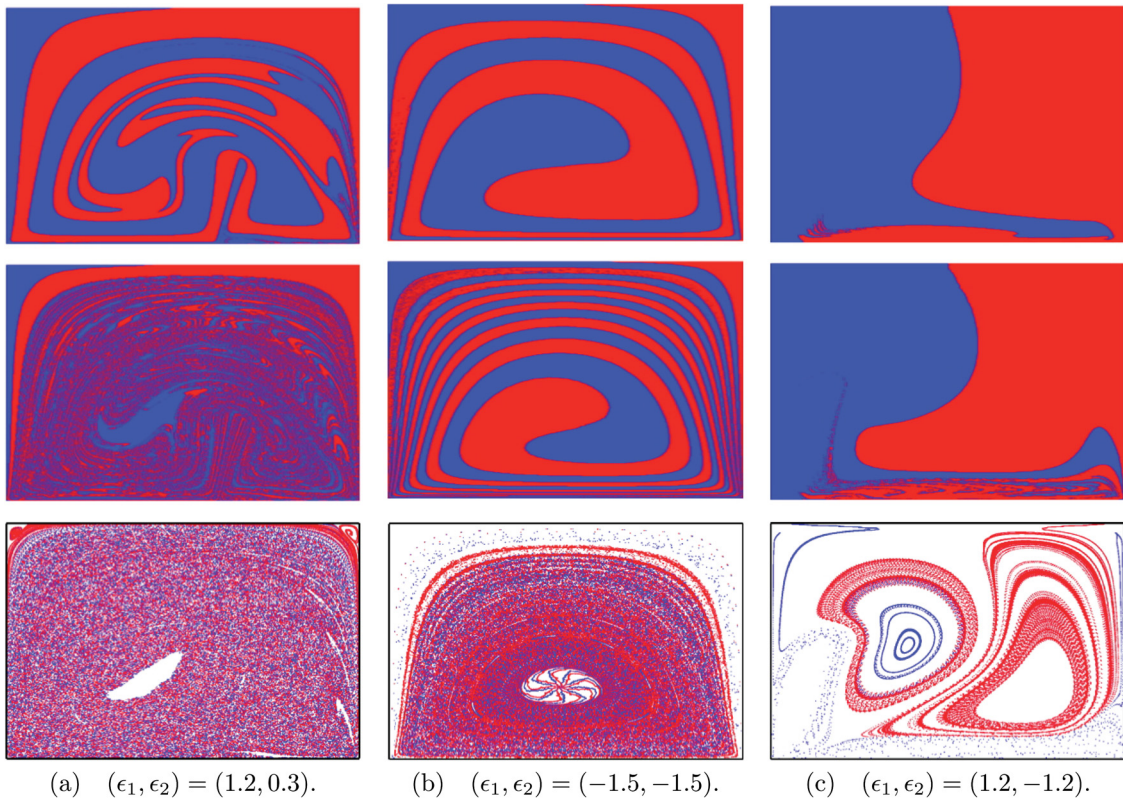


FIG. 10. (Color online) In-In: Species concentrations for (a) a good mixer, (b) a poor mixer with low transversality, and (c) a poor mixer with low transversality and low mobility. Top images: $t = 10$; middle images: $t = 30$; bottom images: Poincaré sections for 10 000 cycles (final $t = 20 000$), seeding 20 particles uniformly along $y = 0.5$.

VII. SUMMARY AND FUTURE WORK

In this paper, we described further advances of Eulerian indicators as predictors of Lagrangian transport phenomena, with a focus on mixing. In particular, we have introduced a new Eulerian indicator, mobility, and applied it to a two-dimensional, lid-driven Stokes flow within a rectangular domain operating in a blinking mode. This flow serves as a model for mixing in a three-dimensional, spatially periodic, steady channel flow, where the blinking two-dimensional flow patterns model the two cross-sectional flow patterns that the fluid experiences as it moves down a spatially periodic channel. The blinking time models the time of flight between the two cross-sectional flow patterns.

We consider two parameters, where each parameter controls the location of a separatrix between two counter-rotating gyres (and, hence, the relative sizes of the two gyres). This two-dimensional design space is then discretized into 10201 equally spaced points, and the transport for each of these points in the design space was computed. For an initial condition with two fluid species (blue and red here) introduced in equal amounts, blue (darker) on the left, red (lighter) on the right, and filling the entire domain, the variance of concentration as a function of time was computed for $0 \leq t \leq 30$. The Eulerian indicator corresponding to transversality (streamline crossing) was computed for the entire design space, and the new Eulerian indicator, mobility, was similarly computed. It was found that the largest values of the product of transversality and mobility correlate well with the smallest values of the variance of concentration at $t = t_f = 30$. This implies that the quality of the (Lagrangian) mixing can be determined from certain Eulerian quantities for the flow studied in this paper.

These Eulerian quantities provide a different insight into mixing behavior and, being Eulerian in nature, may be more amenable to experimental determination. It is also significant that they can be computed directly from the velocity field and do not require the computation of fluid particle trajectories. This results in a significant reduction in computational effort and may prove very useful in the design of complex fluid elements at the micro- and nano-scales. *Finally, this study shows that the best mixing configurations for the blinking, two-dimensional lid-driven flows come from In-In and asymmetric choices in the design space.*

In conclusion, the following broad results come from this study:

1. A systematic search of the design space for two dimensional lid-driven flows has been performed, made possible by employing the CTB to speed up advection calculations.
2. Eulerian indicators have been used to predict optimal mixing configurations, where the product of transversality, α , and the new indicator mobility, η , are shown to correlate well with the variance of concentration, $\mathcal{V}(t_f = 30)$.
3. The optimal designs for this model favor the *In-In* flow configurations.
4. The optimal designs also favor *asymmetric* placements of the separatrices, in contrast to the standard usage for the SHM.

5. The low computational cost of calculating Eulerian indicators enables exploration of a much larger parameter space compared to using traditional modeling. For the current study, calculating the EIs for the entire design space took less computational time than calculating the variance of concentration for a single design using a traditional approach that integrates the particle trajectories.

The path to full three-dimensional calculations will come through applying the two-dimensional lid-driven flows considered here to a Poiseuille flow along a channel. Finally, a full three-dimensional calculation will be employed for comparison to this hybrid scheme. While transitioning from blinking two-dimensional flows to the full three-dimensional channel flows, the Eulerian indicators need to be reformulated to handle a continuously varying velocity field, as particles traveling along the channel no longer see discrete changes in velocity. These approaches are the focus for our future work.

ACKNOWLEDGMENTS

The research of S.W. was supported by ONR Grant No. N00014-01-1-0769, the research of K.M. was supported by ONR Grant No. N00014-09-WR-2-0256, and the research of D.M. and E.O. was supported by ONR Grant Nos. N00014-09-WR-20255 and N00014-10-WX-21393.

- ¹M. Nasir, D. Ateya, D. Burk, J. Golden, and F. S. Ligler, "Hydrodynamic focusing of conducting fluids for conductivity-based biosensors," *Biosens. Bioelectron.* **25**, 1363 (2010).
- ²A. L. Thangawng, P. B. Howell, Jr., J. J. Richards, J. S. Erickson, and F. S. Ligler, "A simple sheath-flow microfluidic device for micro/nanomanufacturing: Fabrication of hydrodynamically shaped polymer fibers," *Lab Chip* **9**, 3126 (2009).
- ³D. Ateya, J. S. Erickson, P. B. Howell, Jr., L. Hilliard, J. Golden, and F. S. Ligler, "The good, the bad, and the tiny: A review of microflow cytometry," *Anal. Bioanal. Chem.* **391**, 1485 (2008).
- ⁴D. R. Mott, P. B. Howell, Jr., J. P. Golden, C. R. Kaplan, F. S. Ligler, and E. S. Oran, "Toolbox for the design of optimized microfluidic components," *Lab Chip* **6**, 540 (2006).
- ⁵D. R. Mott, P. B. Howell, Jr., K. S. Obenschain, and E. S. Oran, "The numerical toolbox: An approach for modeling and optimizing microfluidic components," *Mech. Res. Commun.* **36**, 104 (2009).
- ⁶R. Sturman and S. Wiggins, "Eulerian indicators for predicting and optimizing mixing quality," *New J. Phys.* **11**, 075031 (2009).
- ⁷K. McIlhany and S. Wiggins, "Optimizing mixing in channel flows: Kinematic aspects associated with secondary flows in the cross-section," *Microfluid. Nanofluid.* **10**, 249 (2011).
- ⁸J. M. Ottino, "Mixing, chaotic advection, and turbulence," *Annu. Rev. Fluid Mech.* **22**, 207 (1990).
- ⁹H. Aref, "Stirring by chaotic advection," *J. Fluid Mech.* **143**, 1 (1984).
- ¹⁰D. V. Khakhar, J. G. Franjione, and J. M. Ottino, "A case study of chaotic mixing in deterministic flows: The partitioned pipe mixer," *Chem. Eng. Sci.* **42**, 2909 (1987).
- ¹¹E. Villermaux, A. D. Stroock, and H. A. Stone, "Bridging kinematics and concentration content in a chaotic micromixer," *Phys. Rev. E* **77**, 015301(R) (2008).
- ¹²R. Sturman, J. M. Ottino, and S. Wiggins, *The Mathematical Foundations of Mixing*, Cambridge Monographs on Applied and Computational Mathematics Vol. 22 (Cambridge University Press, Cambridge, 2006).
- ¹³S. Wiggins and J. Ottino, "Foundations of chaotic mixing," *Phil. Trans. R. Soc. London* **362**(1818), 937 (2004).
- ¹⁴J. M. Ottino, S. C. Jana, and V. S. Chakravarthy, "From Reynolds's stretching and folding to mixing studies using horseshoe maps," *Phys. Fluids* **6**(2), 685 (1994).

- ¹⁵A. D. Stroock, S. K. W. Dertinger, A. Ajdari, I. Mezic, H. A. Stone, and G. M. Whitesides, "Chaotic mixer for microchannels," *Science* **295**, 647 (2002).
- ¹⁶J. Aubin, D. F. Fletcher, and C. Xuereb, "Design of micromixers using CFD modelling," *Chem. Eng. Sci.* **60** (8-9), 2503 (2005).
- ¹⁷P. Howell, D. Mott, D. Fertig, C. Kaplan, J. Golden, E. Oran, and F. Ligler, "A microfluidic mixer with grooves placed on the top and bottom of the channel," *Lab Chip* **5**(5), 524 (2005).
- ¹⁸J.-T. Yang, K.-J. Huang, and Y.-C. Lin, "Geometric effects on fluid mixing in passive grooved micromixers," *Lab Chip* **5**(10), 1140 (2005).
- ¹⁹J. Chen and M. A. Strempler, "Topological chaos and mixing in a three-dimensional channel flow," *Phys. Fluids* **21**, 021701 (2009).
- ²⁰H. Song, X.-Z. Yin, and D. J. Bennett, "Optimization analysis of the staggered herringbone micromixer based on the slip-driven method," *Chem. Eng. Res. Des.* **86**, 883 (2008).
- ²¹A. D. Stroock and G. J. McGraw, "Investigation of the staggered herringbone mixer with a simple analytical model," *Philos. Trans. R. Soc. London Ser. A* **362**(1818), 971 (2004).
- ²²J. Ferziger and M. Peric, *Computational Methods for Fluid Dynamics* (Springer-Verlag, New York, 2002).
- ²³M. Funakoshi, "Chaotic mixing and mixing efficiency in a short time," *Fluid Dyn. Res.* **40**, 1 (2008).
- ²⁴P. V. Danckwerts, "The definition and measurement of some characteristics of mixtures," *Appl. Sci. Res. A* **3**, 279 (1952).
- ²⁵P. V. Danckwerts, "Theory of mixtures and mixing," *Research* **6**, 355 (1953).